Journal of Materials Chemistry A

Accepted Manuscript

ROYAL SOCIETY OF CHEMISTRY

www.rsc.org/materialsA

Table of contents entry

Ultra-light and Elastic Graphene Foams with a Hierarchical Structure and High Oil Absorption Capacity

Jie Bai, Anan Zhou, Zhifeng Huang, Jifeng Wu, Hua Bai*, Lei Li*

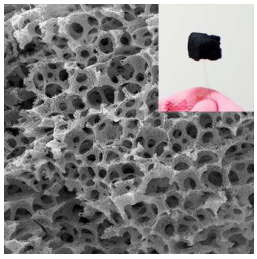

Graphene foams with large cells and excellent elasticity were prepared with mechanical foaming method and used as the oil absorbers.

Journal Name

ARTICLE

Ultra-light and Elastic Graphene Foams with a Hierarchical Structure and High Oil Absorption Capacity†

Received 00th January 20xx,
Accepted 00th January 20xx

DOI: 10.1039/x0xx00000x

www.rsc.org/

Jie Bai, Anan Zhou, Zhifeng Huang, Jifeng Wu, Hua Bai*, Lei Li*

Graphene foams (GFs) have attracted increasing attention because they combine the unique properties of cellular materials and the excellent performance of graphene. The preparation of GFs depends mainly on the self-assembly of graphene or graphene oxide sheets, and designing and controlling the cell morphology of GFs, which determines their properties, remains a challenge. Here, we report a novel strategy for preparing GF with a hierarchical porous structure. Our preparation method involves mechanically foaming a graphene oxide dispersion with the assistance of a surfactant, followed by lyophilization and thermal reduction. These novel GFs possess large cells created using the bubbles as templates and small pores around the edges of the cells resulting from the self-assembly of the graphene oxide sheets. Because of their unique cell structure, the GFs exhibit an ultra-low density, high porosity, good electrical conductivity, and excellent elasticity. In particular, these GFs exhibit a very large absorption capacity (600–1500 g/g) for oils and organic solvents. Our work explores a new strategy for controlling the cell morphology and improving the performance of GFs; the results may shed new light on the relationship between the structure and properties of 3D graphene assemblies.

Introduction

Graphene foams (GFs) are materials with three-dimensional (3D) cellular structures consisting of two-dimensional (2D) graphene nanosheets. They have unique properties as a consequence of their cellular structure, including high porosity and low density, combined with the outstanding merits of graphene, such as a large specific surface area, good electrical conductivity, and high chemical and thermal stabilities.[1-4] Consequently, GFs have found a wide range of applications in energy conversion and storage,[5-8] catalysis,[9,10] sensing,[11,12] and pollution control.[13-15] GFs can be prepared *via* the 3D self-assembly of graphene oxide (GO) or chemically converted graphene (CCG) sheets during hydrothermal reaction, chemical reduction, or direct lyophilization-thermal reduction;[16,17] the typical structure of these GFs is a disordered network of 2D graphene sheets with irregular pores.[18] Although GFs can be prepared efficiently using these methods, the self-assembly of GO and CCG is difficult to control. The properties of a foam are predominantly determined by the intrinsic properties of the material, its porosity and its cell morphologies.[19] In the case of GFs, if the cell size and morphology could be adjusted, the properties of such materials could be optimized to suit a broader range of applications. Therefore, the challenge in developing novel GFs lies in how to control their cell morphologies.

One strategy for manipulating the cell structure of GFs is to use a soft template. Shi *et al*. recently prepared macroporous GFs using organic solvent droplets as templates *via* an improved hydrothermal process.[20] Barg *et al.* also reported the preparation of macroporous GFs from an oil-in-water emulsion containing GO in the aqueous phase.[21] Using these methods, 100–200 μm macropores were constructed in the GFs. The two aforementioned types of macroporous GFs both exhibited good elasticity, and the large pores significantly increased their oil absorption capacity.[21] However, emulsion-based techniques are relatively expensive and complicated because they involve the use of organic solvents, which must subsequently be removed from the as-prepared GFs. For the same reason, these techniques are not eco-friendly. These drawbacks limit the practical application of GFs. In this communication, we report a novel procedure to prepare GFs using air bubbles as templates. In our approach, a GO dispersion is first foamed by a mechanical foaming method[22,23] and subsequently lyophilized and reduced to produce a GF. This procedure typically affords a foam structure with cells larger than 100 μm because of the foaming process, and the walls and edges of the cells are composed of a 3D porous network of CCG sheets. Therefore, the GFs generated *via* our approach exhibit a hierarchical porous structure. These GFs have outstanding properties, including ultra-low density, good electrical conductivity, high porosity, and excellent elasticity. Moreover, we will demonstrate that our GFs exhibit a huge absorption capacity for organic solvents as a consequence of their unique pore structure.

College of Materials, Xiamen University, Xiamen, 361005, P. R. China. E-mail: baihua@xmu.edu.cn; lilei@xmu.edu.cn

† Footnotes relating to the title and/or authors should appear here.
Electronic Supplementary Information (ESI) available: Additional figures and videos as described in the text. See DOI: 10.1039/x0xx00000x

Results and discussion

The preparation of GFs using a mechanical foaming method combined with lyophilization and thermal reduction is illustrated in Fig. 1A. Briefly, a GO dispersion was first mixed with an anionic surfactant, sodium dodecyl sulphate (SDS), which acted as the foaming agent. The blend dispersion was then foamed by vigorous agitation with a mechanical agitator for approximately 1 min, until all of the liquid was converted into a viscous foam. The total volume of the foam was approximately five times as large as that of the original dispersion, as depicted in Fig. 1B. The foamed dispersion was then frozen in liquid nitrogen and lyophilized to yield a GO foam (GOF, Fig. 1D). Finally, the GOF was transferred into a tube furnace and pyrolysed at 400 °C under an argon atmosphere for 2 h. During the pyrolysis, the GOF was converted into a GF (Fig. 1E). GFs prepared using different GO/SDS ratios are referred to as GF*m*-*n*, where *m* and *n* are the concentration of GO and SDS in mg mL^{-1}, respectively. The corresponding GOFs are denoted as GOF*m*-*n*.

A mechanical foaming technique was used in this work to prepare GF. In the mechanical foaming process, the bubbles are generated by mechanical agitation of the solution.[24] Mechanical foaming is a facile method of preparing foams, and has been widely employed in both industry and daily life. One of the most important applications of mechanical foaming is in making cakes, where eggs are foamed by whisking.[25] In our experiments, when the GO/SDS dispersion was agitated, a large volume of air became trapped in the solution, forming numerous bubbles. The microscopic image of the foamed GO/SDS dispersion is shown in Fig. 1C. As evident in this image, the foamed dispersion is a wet foam because the bubbles touch each other and are slightly flattened.[24] The diameters of the bubbles formed are within the range of 50–300 μm. According to the volume ratio between the wet foam and the original dispersion, the liquid volume fraction (ϕ_l) of the foam was approximately 0.2—much smaller than the volume fraction of a liquid with close-packing bubbles (ϕ_l^*), which is 0.36 for a disordered foam.[26] This result also confirms that the foamed GO/SDS dispersion is a wet foam rather than a bubbly solution. A low ϕ_l is important for the preparation of ultra-light GFs.[24]

The as-produced GO/SDS wet foams were stable for several tens of minutes. SDS plays a critical role in the foaming process. We observed that pure GO dispersions were not foamable under our experimental conditions. The bubbles in the pure GO dispersion ruptured quickly after they were generated. From a thermodynamic point of view, a foamable solution should have a relatively low surface tension. As shown in Fig. 2, the GO did not decrease the surface tension of water. The surface tension of the GO dispersions was measured to be 72–73 mN m^{-1}—very similar to the value of pure water (72.4 mN m^{-1} for the water used in our experiments)—and was independent of the concentration of GO. A possible explanation for these results is that the adsorption of GO

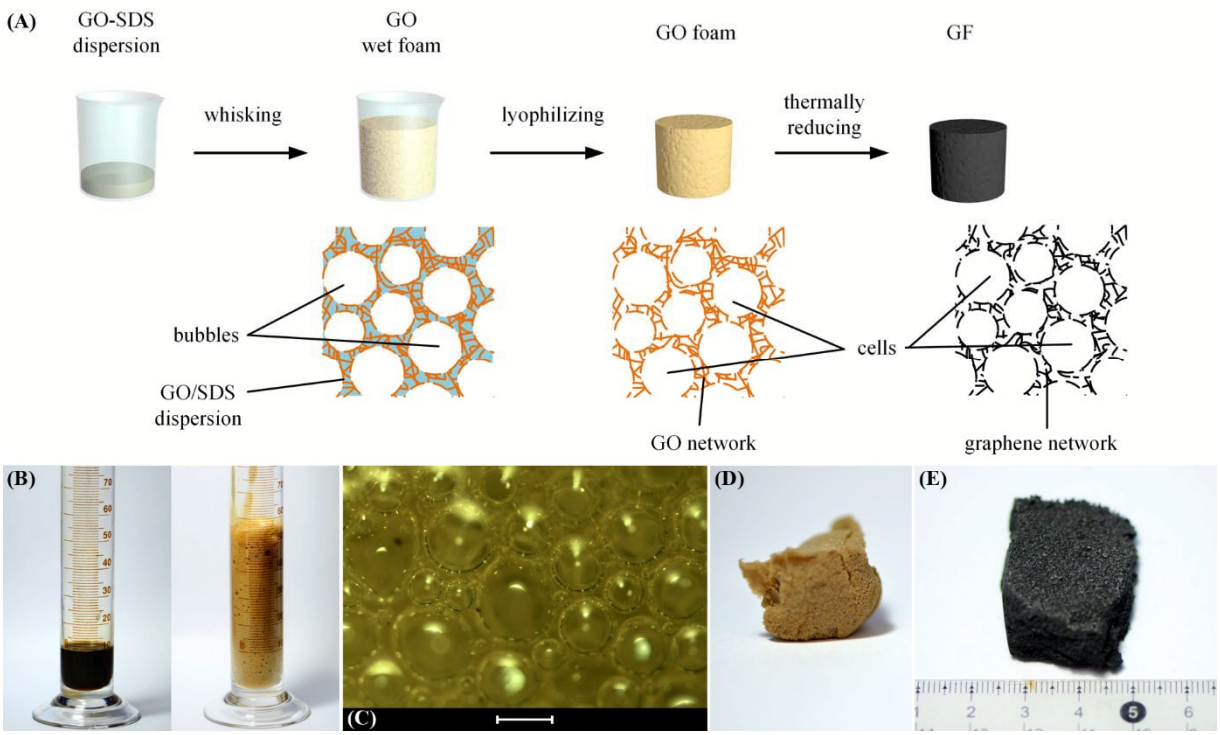

Fig. 1. Preparation and photographs of GFs. (A) Preparation of GFs by mechanical foaming combined with lyophilization and thermal reduction. (B) Photograph of a GO dispersion (left) and a GO wet foam (right). (C) Microscopic photograph of a GO wet foam. Scale bar: 200 μm. (D) Photograph of GOF5-1. (E) Photograph of GF5-1.

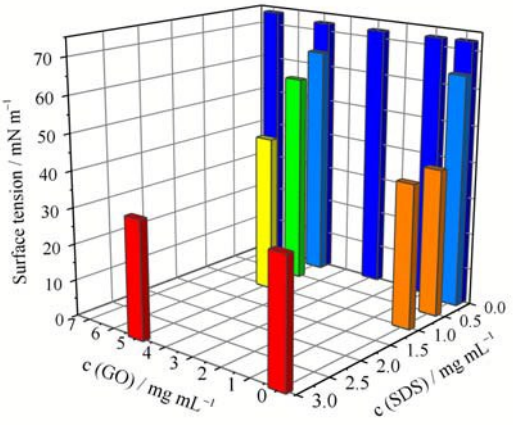

Fig. 2. Surface tension of different GO/SDS blend dispersions.

sheets at the interface is too slow. In the surface tension measurements, the adsorption equilibrium of GO at the interface is assumed to have been established beforehand.[27] However, the diffusion of GO sheets in water should be quite slow because of their large size.[28] Therefore, in the time scale of our experiments, GO sheets could not diffuse to the liquid/gas interface and reduce the surface tension of water. When SDS was added to a 5 mg mL^{-1} GO dispersion, the surface tension decreased significantly: from 72.2 mN m^{-1} for a pure GO dispersion to 43.2 mN m^{-1} for a GO dispersion containing 1 mg mL^{-1} SDS. As a result, all the GO/SDS blend dispersions were foamable, except for the one containing 0.1 mg mL^{-1} SDS. Its surface tension of 64.2 mN m^{-1} was still too high to foam. The surface-tension measurements clearly demonstrate the importance of SDS in the foaming process.

Notably, as shown in Fig. 2, the surface tension of the GO/SDS dispersion is higher than that of the corresponding pure SDS solution at the same SDS concentration. This greater surface tension of the GO/SDS dispersion becomes obvious when the concentration of SDS is low. For example, the surface tension of the GO/SDS dispersion containing 0.5 mg mL^{-1} SDS was 58.0 mN m^{-1}, whereas that of a 0.5 mg mL^{-1} SDS solution was only 40.4 mN m^{-1}. The reason for this discrepancy is that a great number of SDS molecules adsorb onto the surface of the GO sheets *via* the hydrophobic interaction between the alkyl chains of SDS and the conjugated regions of the GO sheets.[29] This adsorption competes with the interfacial adsorption, leading to the increase of the surface tension. At this point, GO is detrimental to the foamability of the blend dispersion. However, from a kinetics viewpoint, GO contributes to the stability of the wet foam because GO can slow the drainage of the wet foam. Drainage is the passage of liquid through the foam. Gravity-driven drainage will lead to the separation of bubbles and liquid in the wet foam: the liquid flows downwards, and the gas bubbles are displaced upwards. The drainage of a foam, in the simplest model, is treated as the passage of the liquid through a porous medium, and the flux (u_m) through the foam is described by Darcy's law:[24]

$$u_m \boldsymbol{e} = \frac{\alpha}{\eta}\left(\rho_l \boldsymbol{g} - \nabla p\right),$$

where $\boldsymbol{e}$ is the unit vector of the flow direction, α is the permeability coefficient of the liquid foam, which is related to the structure of the foam, η is the viscosity of the liquid, ρ_l is the density of the liquid, $\boldsymbol{g}$ is the acceleration due to gravity, and p is the pressure that forces the flowage of the liquid. We observed that the viscosity of the 1 mg mL^{-1} SDS solution was 2 Pa s; however, when GO (5 mg mL^{-1}) was incorporated into the dispersion, the viscosity increased substantially to 20 Pa s. Therefore, the u_m is expected to be 10 times lower, leading to a markedly slowed drainage.

The GO/SDS wet foams were lyophilized to produce solid GOFs. Lyophilization can remove water from the wet foams while preserving the foam structure. GOFs were then reduced by thermal treatment at 400 °C under an argon atmosphere to yield GFs (see Fig. S1A for the thermogravimetic analysis (TGA) curve of GOF).[30,31] The reduction of GO was confirmed by X-ray photoelectron spectroscopy (XPS) (Fig. S2), where the C–O component of the C 1s line in the XPS spectrum became very small after the thermal treatment. Also the intensity ratio of D/G bands in Raman spectra (Fig. S3) increased after the thermal treatment, demonstrating the reduction of GO. Fig. 3 depicts scanning electron microscopy (SEM) images of GOF5-1 and GF5-1. The morphologies of GOF5-1 and GF5-1 are similar, suggesting that the thermal treatment did not significantly alter the foam structure. Both GOF5-1 and GF5-1 exhibit the characteristic morphology of a solid foam, with ample closely packed large cells. The diameters of the cells range from 100 to several hundred micrometres, in agreement with the

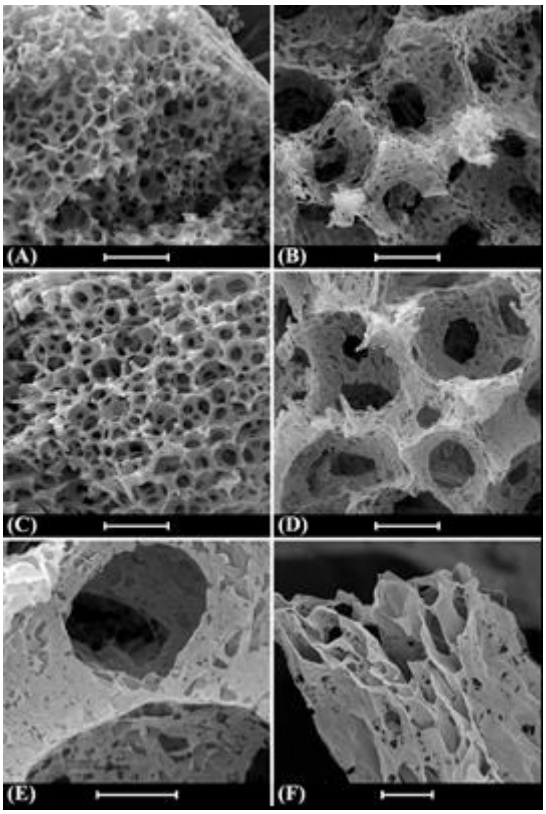

Fig. 3. SEM images of GOF5-1 and GF5-1. GOF5-1 (A, B) and GF5-1 (C–F). Scale bar: (A, C) 500 μm, (B, D) 100 μm, (E) 50 μm, (F) 10 μm.

bubbles formed in the GO/SDS wet foams. Clearly, the structure of the wet foam is well preserved in the solid GOFs and GFs. Moreover, along the faces and edges of the cells in the solid foams, a 3D network consisting of 2D GO or CCG sheets is observed. Such network structures are characteristic of GO or CCG aerogels,[18] and were generated by the self-assembly of GO sheets on the faces and edges of the wet foams. Because GO sheets have a large lateral size and high mechanical strength, when a GO dispersion is lyophilized, the GO sheets can prop each other up to form a 3D network.[32] Therefore, the GOFs and GFs have a hierarchical porous structure that consists of large cells templated from bubbles, and small pores between GO or CCG sheets on the faces and edges.

Interestingly, we observed that the foaming process induced the formation of new self-assembled structures of GO in the foam. As shown in Fig. 3E, the GO sheets at the surface of the cells are parallel to the surface, indicating that they are adsorbed at the gas/liquid interface in the wet foam. This observation is attributed to the surface activity of GO.[28,33] Although the diffusion of GO sheets in the dispersion is quite slow, the adsorption equilibrium of GO at the interface will be achieved finally in the wet foam after a sufficiently long period. This GO adsorbed layer may further improve the stability of the bubbles. Another unique feature observed in these solid foams is the orientation of GO sheets along the axes of the edges of the cells. This orientation is caused by the liquid flow at the edges. Liquid flow always exists in wet foams. It occurs along the axial directions of the edges and is driven by gravity (self-drainage) or by the pressure difference caused by the different curvature of the gas/liquid interfaces (capillary suction, as suggested by the Young-Laplace law).[24] Meanwhile, GO sheets have been reported to tend to form a liquid-crystal phase at concentrations as low as 1 mg mL^{-1} because of their high asymmetry.[34-36] As a result, the flow in the wet foam will induce the formation of a GO liquid-crystal phase in which GO sheets are parallel to the flow direction.

We further investigated the influence of the concentrations of GO and SDS on the morphology of the GFs. For blend dispersions containing 5 mg mL^{-1} GO and variable SDS (> 0.5 mg mL^{-1}, to ensure the foamibility of the blend dispersion), the concentration of SDS had little effect on the morphology of the final GFs, as shown in Fig. S4. However, the concentration of GO determines the morphology of the GFs. As previously discussed, wet foams could be prepared with 1 mg mL^{-1} SDS, independent of the GO concentration; however, not all the wet foams could be converted into a GOF and a GF. When the GO concentration was 1 mg mL^{-1}, no intact foam structure was observed after the wet foam was lyophilized, except for some disordered GO sheets, as shown in **Fig. 4**A and B (the SEM images of the corresponding GOFs are shown in Fig. S5). These results arise because, at low concentrations, the quantity of GO sheets is not sufficient to form a stable network after lyophilization; thus, the cellular structure of the foam collapses.[32] When the GO concentration was increased to 3 mg mL^{-1} (GF3-1, Fig. 4C and D), the typical hierarchical foam

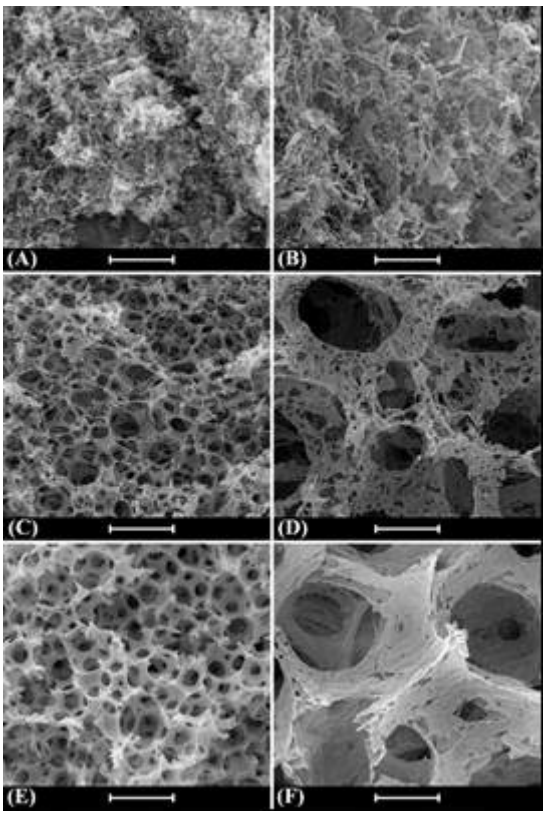

Fig. 4. SEM images of different GFs: (A, B) GF1-1; (C, D) GF3-1; (E, F) GF7-1. Scale bar: (A, C, E) 500 μm; (B, D, F) 100 μm.

structure was obtained. Compared to GF5-1, GF3-1 contains more pores on the faces and edges of the cells, which is a consequence of fewer GO sheets being necessary to construct the foam. As expected, further increasing the concentration of GO to 7 mg mL^{-1} (GF7-1) led to a foam with more compact faces and edges, as depicted in Fig. 4E and F.

The density of the GFs is quite low. Fig. 5A shows that a GF5-1 monolith with the volume of ~2.5 cm^3 could be supported by a single human hair. The typical density of GF5-1 was ~0.8 mg cm^{-3}. For comparison, the typical density of a graphene aerogel (GAG) is approximately 10 ~ 30 mg cm^{-3}.[10,21] Clearly, the large cells efficiently lower the density of the GF. The porosity of GF5-1 was calculated to be 99.96% on the basis of the apparent density of the foam (with a specific surface area of 134.2 m^2 g^{-1}). Notably, the liquid fraction (ϕ) of the GO/SDS wet foam is 0.2, which corresponds to a porosity of 80%. Therefore, the additional pore volume originates from the 3D network structure of the edges in the foam, and both the large cells and small pores contribute to the low density of the foam. In previous investigations, to decrease the density of GAG, the feeding amount of GO or CCG sheets was frequently reduced so that the walls of the pores in the GAGs could be thinner. With this method, the density of GAG will reach a limit when the walls are so thin that they fail to support the network. However, our strategy of introducing large cells can further reduce the density of the GFs beyond this limit. We also measured the electrical properties of the prepared GFs. As depicted in Fig. 5B, the current-voltage (I-V) curve of a GF5-1 monolith is a straight line, which is the characteristic I-V

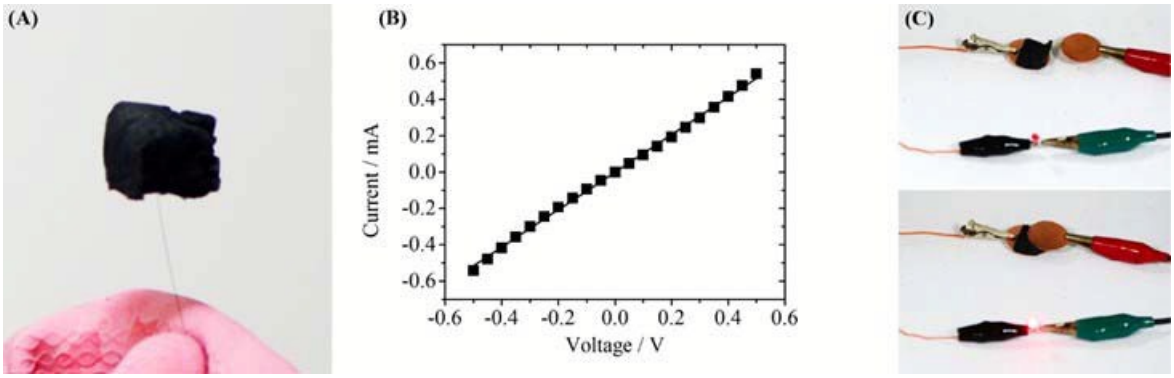

Fig. 5. Physical properties of GF5-1. (A) Photograph of a GF5-1 monolith (~2.5 cm^3) supported by one human hair. (B) Current-voltage curve of a GF5-1 monolith. (C) Photographs of a circuit with an LED and a GF5-1 monolith to demonstrate that the GF5-1 is conductive.

behaviour of a resistor. The apparent conductivity of GF5-1 was measured to be 10^{-2} S m^{-1}. This value is lower than that of GAG (10^{-1} S m^{-1})[16] because of the larger porosity of the GF. As shown in Fig. 5C, an LED was illuminated when a GF monolith was connected in a circuit. Therefore, the GFs can be used as an ultra-light and soft conductor in many applications.

The GFs exhibit good mechanical elasticity. As shown in Fig. 6A (a–c), the GF5-1 monolith could return to its original shape and volume after it was compressed to 45% and released (Movie S1). When the monolith was compressed to a larger strain (90%), it could not recover spontaneously (Fig. 6A (d, c)); however, when the compressed monolith was soaked in methanol, it immediately swelled and returned to its original shape, as shown in Fig. 6A (f) (Movie S2). These results demonstrate that the structure of GFs is robust and not damaged even under a large strain. Usually, GO and CCG aerogels are plastic, and, when they are compressed, a large permanent deformation is usually observed. Thus, this work

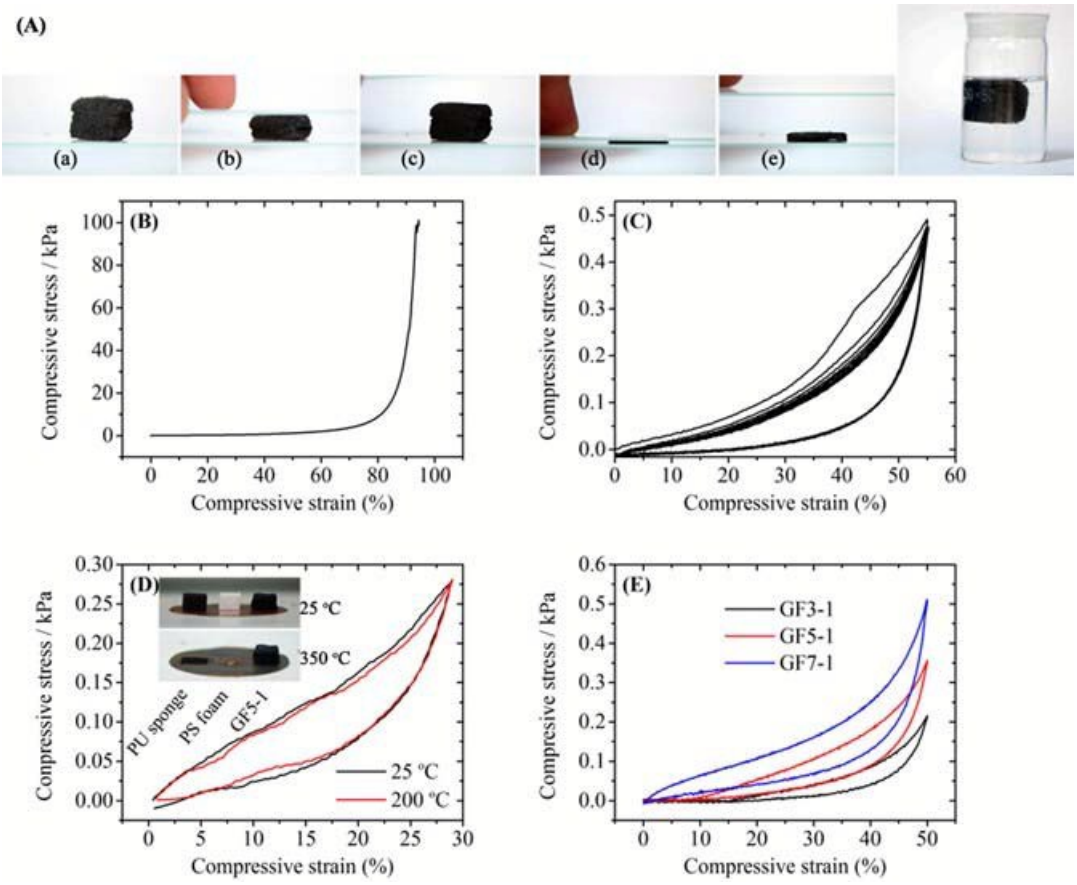

Fig. 6. Mechanical properties of the GFs**.** (A) (a)–(c) A GF5-1 monolith compressed to a strain of 45% and released. (d)–(e) The same monolith compressed to a strain of 90% and released. (f) The above compressed monolith after being soaked in ethanol. (B) Compressive stress-strain curve of GF5-1 over a wide strain range (0–95%). (C) Cyclic compressive stress-strain curves for GF5-1. (D) Comparison of the compressive stress-strain curves for GF5-1 measured at 25 °C and 200 °C. Inset: photographs of a PU sponge, PS foam and GF5-1 at 25 and 350 °C. (E) Compressive stress-strain curves for GFs prepared with GO dispersions of different concentration

establishes a new route to prepare compressible elastic CCG-based porous materials. To investigate the mechanical properties of GFs thoroughly, we performed compression tests. Fig. 6B shows the compressive stress-strain curve for GF5-1 over a large strain range (0–95%). In the strain range of 0–60%, a long plateau is observed where the compressive stress is smaller than 1 kPa and increases very slowly with increasing strain. With a further increase in the strain, the stress begins to grow steeply, reaching 100 kPa at a strain of 95%. This curve is similar to the compressive stress-strain curves of elastomeric foams, such as polyurethane foams.[37] The plateau is caused by buckling of the edges parallel to the direction of compression, and the steeply rising stress observed under a large strain is the result of the densification of the foam. Given that the CCG sheets are rather flexible, buckling of the edges of the cells should not cause fracture of the sheets. Moreover, the CCG sheets on the edges are parallel to each other, thus the $\pi-\pi$ interactions between them are strong. As a result, under compression, the GF monoliths undergo a reversible elastic deformation. However, under a large strain, the foam is densified and some CCG sheets are forced to contact each other. The additional binding interaction between these CCG sheets will prevent the foam from recovering. Ethanol eliminates the binding interaction by intercalating between the CCG sheets and solvating them, thus promoting the recovery of the foam.

The cyclic compressive stress-strain curves for GF5-1 are represented in Fig. 6C, which clearly demonstrates that the GF5-1 is elastic. In the loading curve of the first cycle, a keen point at a strain of 40% is observed. This keen point disappears in the following cycles and is therefore attributed to the irreversible failure of some weaker structures present in the foam, such as slippage of inefficiently stacked CCG sheets. Similar phenomena have been observed for other GFs.[21] The damage of the unstable structures also explains the small dimensional loss during the cyclic compressive test (~9%). All the unloading curves are identical, indicating that the energy stored in the foam is the same in each cycle. The compression test was also performed at a higher temperature to evaluate the thermal stability of the foam. At 350 °C, polymeric foams such as a polyurethane sponge and polystyrene foams melted, but the GF remained unchanged, as depicted in Fig. 6D. The TGA curve (Fig. S1B) reveals that GF5-1 has a high decomposition temperature of 420 °C. Moreover, the compressive curves for GF5-1 at 25 and 200 °C are identical, as shown in Fig. 6D, which demonstrates that the GFs exhibit excellent thermal stability. The high thermal stability of CCG sheets and the strong interactions between them endow the GFs with thermo-insensitive elasticity. These experiments reveal that GFs may have potential applications as high-temperature elastic porous materials.

The mechanical strength of the foams was observed to be dependent on the concentrations of both GO and SDS. As shown in Fig. 6E, the compressive stress of GF3-1 is smaller than those of GF5-1 and GF7-1 at the same strain. Clearly, more CCG sheets on the edges of the foam can improve its mechanical strength. Similarly, a higher SDS concentration also results in a stronger foam (Fig. S6) because SDS is also carbonized during the pyrolysis, as demonstrated by the thermogravimetric analysis curve of SDS and the XPS of the residue (Fig. S8 and S9). The residual carbon generated from the SDS on the edges and faces of the cells also strengthens the structure of the foam.

One important application of porous materials is the absorption of oils.[13,38,39] Pollution produced by oil spills and organic chemical leakage has attracted great attention, and various porous materials have been designed to remove these liquids by absorption. The GFs exhibit high porosity and contain interconnected open pores; they should therefore be excellent candidates for oil absorbents. As illustrated in Fig. 7A,

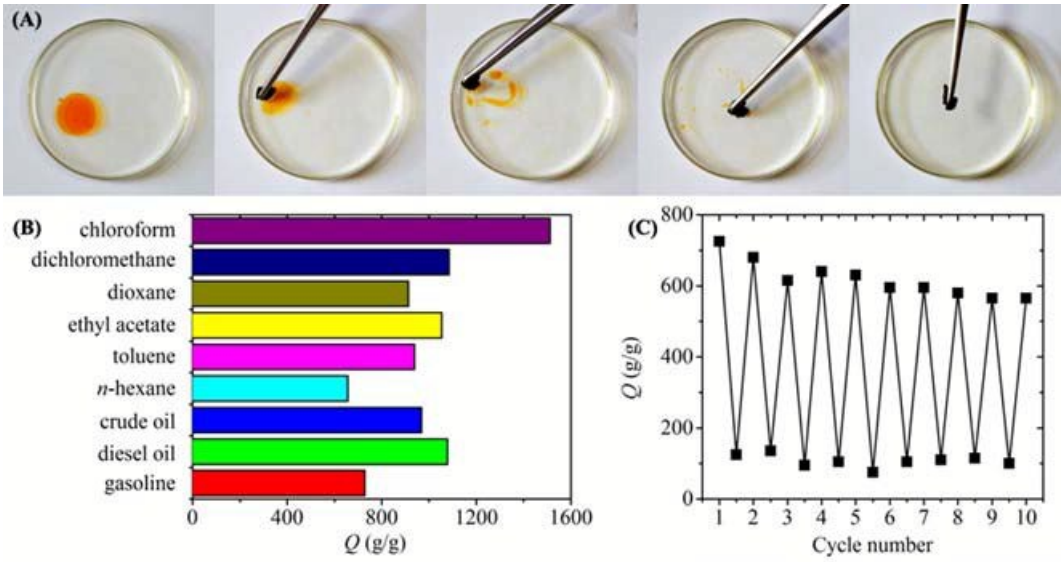

Fig. 7. Oil absorption tests of GF5-1. (A) Absorption process of toluene (stained with an organic dye) on water by the GF5-1. (B) Absorption capacities (*Q*) of GF5-1 towards different organic compounds. (C) Absorption capacities (*Q*) of GF5-1 during the repeated absorption and release of *n*-hexane

the toluene floating on the surface of water was quickly absorbed by a small piece of a GF5-1 monolith, demonstrating the good oil-absorbing ability of the GFs. The absorption capacity of an oil absorbent can be evaluated by *Q*, which is defined as the ratio between the weight after full absorption and the initial weight. Fig. 7B shows the *Q* values of GF5-1 towards several oils and organic solvents. The *Q* values range from 600 to 1500, depending on the density of the solvent. For example, the *Q* value of GF5-1 towards toluene is 938 g/g, which is much higher than that of graphene/carbon nanotube composite aerogels (~350 g/g)[13] and nitrogen-doped graphene frameworks (~210 g/g).[15] To the best of our knowledge, 938 g/g is the highest *Q* value reported in the literature. A detailed comparison between the GFs and other oil absorbents in the literature is provided in Table S1. The large *Q* values are attributed to the unique structure of the GFs prepared here. Compared to conventional GAGs, GFs exhibit lower densities and can absorb and store more solvent in their large cells to achieve a higher absorption capacity. The oils and solvents in the GFs can be released by squeezing or heating. Squeezing or heating will lead to the shrinkage of the GFs; however, upon contact an organic solvent, the shrunken GFs absorb the solvent rapidly and swell within 5 s because of their good elasticity. As shown in Fig. 7C, after repeated absorption and release of *n*-hexane by being squeezed 10 times, GF5-1 still exhibited a *Q* value of 565 g/g. Therefore, because of their strong oil-absorbing performance, GFs are expected to be promising oil sorbents with potential applications in pollution control.

Conclusions

We have devised a novel strategy to fabricate GFs by the mechanical foaming of a GO/SDS dispersion followed by lyophilization and thermal reduction. The GFs have hierarchical porous structures that consist of large cells generated by mechanical foaming, and small pores on the faces and edges of the cells formed as a consequence of the self-assembly of the GO sheets. Further investigations confirmed that, although a pure GO dispersion is not foamable because GO cannot lower the surface tension, GO sheets can improve the stability of the SDS foam by increasing the viscosity. In addition, the GO sheets in the wet foam exhibit previously undescribed self-assembly behaviour. The GFs exhibit ultra-low densities (< 1 mg cm^{-3}), high porosity, excellent elasticity and good electrical conductivity. The absorption capacity of GF5-1 for various oils and organic solvents was 600–1400, which is much higher than those reported previously for carbon-based absorbents. This work establishes a new method to control the cell morphology of GFs and thereby to prepare a novel class of graphene foam materials. These GFs will find broad applications in environmental protection, energy storage and bioengineering. Additionally, we believe the results presented in this work may shed new light on the relationship between the structure and properties of 3D graphene assemblies.

Experimental

Materials

GO was prepared by the oxidation of natural graphite powder (325 mesh, Qingdao Huatai Lubricant Sealing S&T Co., Ltd.) according to a modified Hummers' method. Diesel (90#) and gasoline (93#) used in the experiments are the products of the China National Petroleum Corporation. The density of the crude oil was 0.74 g L^{-1}.

Preparation of GF

The preparation of GF upon mechanical foaming is illustrated in Fig. 1A. Typically, a GO aqueous dispersion (1–7 mg mL^{-1}) containing SDS (0.5–3 mg mL^{-1}) was subjected to vigorous agitation with a mechanical agitator for 1 min at a speed of 1000 rpm, until the volume of the foam stopped to increase. The foamed dispersion was then then transferred into a steel container and lyophilized for 24 h to yield a GOF. Finally, the GOFs were pyrolysed at 400 °C in a tube furnace under an argon atmosphere for 2 h to produce GFs.

Oil absorption tests

The oil absorption capacity of GF5-1 was measured for various organic compounds with different densities, including chloroform, dichloromethane, dioxane, ethyl acetate, toluene, n-hexane, crude oil, diesel fuel, and gasoline. A GF5-1 monolith with a volume of ~3 cm^3 was used for each absorption test. The weights before and after absorption were recorded by an electronic balance. In the cyclic absorption experiments, the GF5-1 was squeezed to release the absorbed solvents.

Characterization

The morphology of the composites was observed using a field-emission scanning electron microscope (LEO 1530) operated at 20 kV. X-ray photoelectron spectroscopy (XPS) was performed on a PHI Quantum 2000 spectrometer using monochromated X-rays from an Al-Kα source with a take-off angle of 45° from the surface plane. Surface tension was measured on a DCAT21 surface tensiometer (Dataphy Instruments Co., Ltd.). The compressive tests were carried out at a rate of 100% strain min^{-1} using a model 3342 Instron universal testing machine.

Acknowledgements

This work was financially supported by the National Natural Science Foundation of China (21104041, 21444004).

Notes and references

1 K. S. Novoselov, V. I. Fal'ko, L. Colombo, P. R. Gellert, M. G. Schwab and K. Kim, *Nature*, 2012, **490**, 192-200.
2 A. K. Geim, *Science*, 2009, **324**, 1530-1534.
3 C. N. R. Rao, A. K. Sood, K. S. Subrahmanyam and A. Govindaraj, *Angew. Chem. Int. Ed.*, 2009, **48**, 7752-7777.
4 M. J. Allen, V. C. Tung and R. B. Kaner, *Chem. Rev.*, 2010, **110**, 132-145.
5 Y. Xu, Z. Lin, X. Huang, Y. Wang, Y. Huang and X. Duan, *Adv. Mater.*, 2013, **25**, 5779-5784.
6 Z. S. Wu, A. Winter, L. Chen, Y. Sun, A. Turchanin, X. Feng and K. Müllen, *Adv. Mater.*, 2012, **24**, 5130-5135.
7 L. Zhang and G. Q. Shi, *J. Phys. Chem. C*, 2011, **115**, 17206-17212.
8 J. Chen, K. Sheng, P. Luo, C. Li and G. Shi, *Adv. Mater.*, 2012, **24**, 4569-4573.
9 C. Hu, H. Cheng, Y. Zhao, Y. Hu, Y. Liu, L. Dai and L. Qu, *Adv. Mater.*, 2012, **24**, 5493-5498.
10 Z. Tang, S. Shen, J. Zhuang and X. Wang, *Angew. Chem. Int. Ed.*, 2010, **49**, 4603-4607.
11 C. Du, Z. Yao, Y. Chen, H. Bai and L. Li, *RSC Adv.*, 2014, **4**, 9133-9138.
12 L. Chen, X. Wang, X. Zhang and H. Zhang, *J. Mater. Chem.*, 2012, **22**, 22090-22096.
13 H. Sun, Z. Xu and C. Gao, *Adv. Mater.*, 2013, **25**, 2554–2560.
14 Y. Q. Chen, Q. K. Zhang, L. B. Chen, H. Bai and L. Li, *J. Mater. Chem. A*, 2013, **1**, 13101-13110.
15 Y. Zhao, C. Hu, Y. Hu, H. Cheng, G. Shi and L. Qu, *Angew. Chem. Int. Ed.*, 2012, **51**, 11371-11375.
16 Y. X. Xu, K. X. Sheng, C. Li and G. Q. Shi, *ACS Nano*, 2010, **4**, 4324-4330.
17 H. Bi, K. Yin, X. Xie, Y. Zhou, N. Wan, F. Xu, F. Banhart, L. Sun and R. S. Ruoff, *Adv. Mater.*, 2012, **24**, 5124–5129.
18 C. Li and G. Shi, *Adv. Mater.*, 2014, **26**, 3992-4012.
19 L. J. Gibson and M. F. Ashby, *Cellular Solids: Structure and Properties*, Cambridge University Press, Cambridge, UK, 1999.
20 Y. Li, J. Chen, L. Huang, C. Li, J. D. Hong and G. Shi, *Adv. Mater.*, 2014, **20**, 4789–4793.
21 S. Barg, F. M. Perez, N. Ni, P. do Vale Pereira, R. C. Maher, E. Garcia-Tuñon, S. Eslava, S. Agnoli, C. Mattevi and E. Saiz, *Nat. Commun.*, 2014, **5**, 4328.
22 T. Tomita, S. Kawasaki and K. Okada, *J. Porous Mater.*, 2004, **11**, 107-115.
23 Y. Yang, S. Z. Shimai, Y. Sun, M. J. Dong, H. Kamiya and S. W. Wang, *J. Mater. Res.*, 2013, **28**, 2012-2016.
24 I. Cantat, S. Cohen-Addad, F. Elias, F. Graner, R. Höhler, O. Pitois, F. Rouyer and A. Saint-Jalmes, *Foams: Structure and Dynamics*, Oxford University Press, Oxford, UK, First edn., 2010.
25 A. H. Massey, A. S. Khare and K. Niranjan, *J. Food Sci.*, 2001, **66**, 1152-1157.
26 F. A. L. Dullien, *Porous Media. Fluid Transport and Pore Structure*, Academic Press, Waltham, Massachusetts, USA, second edn., 1992.
27 J. Eastoe and J. S. Dalton, *Adv. Colloid Interface Sci.*, 2000, **85**, 103-144.
28 J. Kim, L. J. Cote, F. Kim, W. Yuan, K. R. Shull and J. Huang, *J. Am. Chem. Soc.*, 2010, **132**, 8180-8186.
29 M. Lotya, Y. Hernandez, P. J. King, R. J. Smith, V. Nicolosi, L. S. Karlsson, F. M. Blighe, S. De, Z. Wang, I. T. McGovern, G. S. Duesberg and J. N. Coleman, *J. Am. Chem. Soc.*, 2009, **131**, 3611-3620.
30 H. C. Schniepp, J. L. Li, M. J. McAllister, H. Sai, M. Herrera-Alonso, D. H. Adamson, R. K. Prud'homme, R. Car, D. A. Saville and I. A. Aksay, *J. Phys. Chem. B*, 2006, **110**, 8535-8539.
31 S. Pei and H.-M. Cheng, *Carbon*, 2012, **50**, 3210-3228.
32 H. Bai, X. L. Wang, C. Li and G. Q. Shi, *J. Phys. Chem. C*, 2011, **115**, 5545–5551.
33 L. J. Cote, F. Kim and J. Huang, *J. Am. Chem. Soc.*, 2008, **131**, 1043-1049.
34 Z. Xu, H. Sun, X. Zhao and C. Gao, *Adv. Mater.*, 2013, **25**, 188-193.
35 J. E. Kim, T. H. Han, S. H. Lee, J. Y. Kim, C. W. Ahn, J. M. Yun and S. O. Kim, *Angew. Chem. Int. Ed.*, 2011, **50**, 3043-3047.
36 X. Lei, Z. Xu, H. Sun, S. Wang, C. Griesinger, L. Peng, C. Gao and R. X. Tan, *J. Am. Chem. Soc.*, 2014, **136**, 11280-11283.
37 L. J. Gibson and M. F. Ashby, *Cellular Solids: Structure and Properties*, Cambridge University Press, Cambridge, UK, 1997.
38 A. J. Zhang, M. J. Chen, C. Du, H. Z. Guo, H. Bai and L. Li, *ACS Appl. Mater. Interfaces*, 2013, **5**, 10201-10206.
39 H. Zhao, X. Song and H. Zeng, *NPG Asia Mater.*, 2015, **7**, e168.